



Contents lists available at ScienceDirect

Spectrochimica Acta Part A: Molecular and Biomolecular Spectroscopy

journal homepage: www.journals.elsevier.com/spectrochimica-acta-part-a-molecular-and-biomolecular-spectroscopy

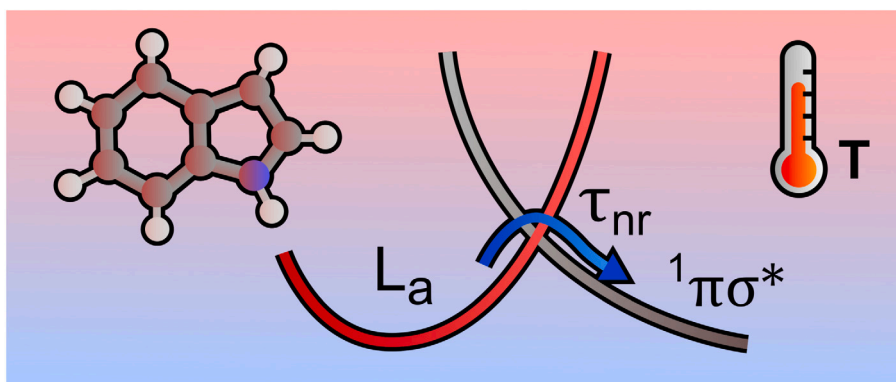
Modeling the temperature dependence of the fluorescence properties of Indole in aqueous solution

Cheng Giuseppe Chen^a, Andrea Amadei^b, Marco D'Abramo^{a,*}^a Department of Chemistry, Sapienza University of Rome, Piazzale Aldo Moro, 5, Rome, 00185, Italy^b Department of Technological and Chemical Sciences, Tor Vergata University of Rome, Via della Ricerca Scientifica, 1, Rome, 00133, Italy

HIGHLIGHTS

- Reproduced the temperature dependence of the Indole fluorescence properties in H₂O.
- Applied recent QM/MM-based approach to model electronic transitions suitable for rare events.
- Higher water fluctuations at higher temperatures increase the rate of the $^1L_b \rightarrow ^1\pi\sigma^*$ and $^1L_a \rightarrow ^1\pi\sigma^*$ transitions.
- The thermodynamic properties of the $^1L_b \rightleftharpoons ^1L_a$ interconversion were estimated.

GRAPHICAL ABSTRACT



ARTICLE INFO

Keywords:

Indole
Fluorescence
MD-PMM
Excited state dynamics
Temperature dependence

ABSTRACT

In a recent paper, we proposed a scheme to describe the relaxation mechanism of the excited Indole in aqueous solution, involving the fluctuations among the diabatic electronic states 1L_b , 1L_a and $^1\pi\sigma^*$. Such a theoretical and computational model reproduced accurately the available experimental data at room temperature. Following these results, in the present work, we model the complex temperature dependence of the fluorescence properties of Indole in aqueous solution, with results further validating the proposed relaxation scheme. This scheme is able to explain the temperature effects on the fluorescence behavior indicating the water fluctuations as the main cause of (i) the stabilization of the dark state ($^1\pi\sigma^*$) and (ii) the increase in temperature of the kinetics of the irreversible transition towards such a state.

1. Introduction

Over the years, Indole has been the subject of numerous studies – both experimental [1–6] and theoretical [7–14] – as the model system for the absorption and emission properties of the amino acid tryptophan (Trp). This interest arises from the unique spectroscopic properties of Trp, which are largely dependent on the polarity of its surrounding environment and have been successfully exploited to gain structural and dynamic information on proteins [15–19]. This marked sensitivity

towards its environment is rather complex and it is often hard to provide a quantitative interpretation at the atomistic level. Such a complexity arises from the interplay between two singlet diabatic electronic states, 1L_b and 1L_a , hereafter termed as L_b and L_a , determining the electronic character of the Indole electronic first excited eigenstate: the former corresponding to the gas phase first electronic excited eigenstate as obtained at the ground eigenstate geometry and the latter, a gas phase higher energy electronic eigenstate, greatly stabilized by the

* Corresponding author.

E-mail addresses: andrea.amadei@uniroma2.it (A. Amadei), marco.dabramo@uniroma1.it (M. D'Abramo).<https://doi.org/10.1016/j.saa.2024.124096>

Received 16 October 2023; Received in revised form 5 February 2024; Accepted 27 February 2024

Available online 28 February 2024

1386-1425/© 2024 The Authors. Published by Elsevier B.V. This is an open access article under the CC BY license (<http://creativecommons.org/licenses/by/4.0/>).

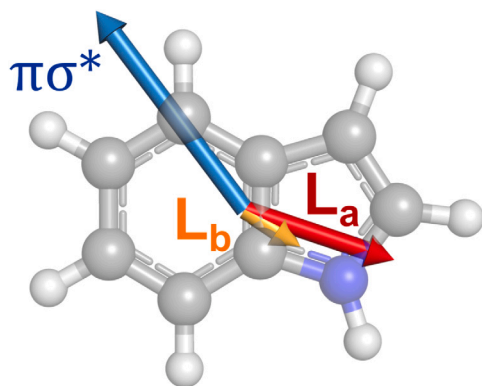


Fig. 1. Graphical representation of the Indole molecule (H in white, C in gray and N in blue). The electric dipole moments of the L_b (orange), L_a (red) and $\pi\sigma^*$ (blue) states (calculated using EOM-CCSD/6-311+G(d) at the geometry corresponding to the gas phase electronic ground eigenstate energy minimum) are also shown.

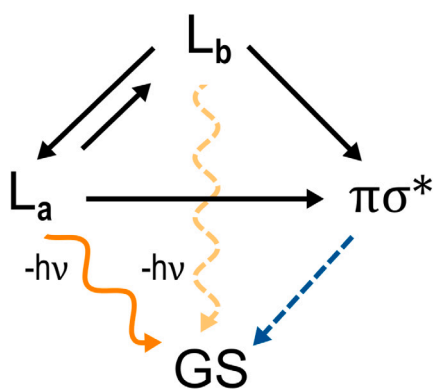


Fig. 2. Scheme representing our proposed relaxation mechanism of aqueous Indole [14].

solvent (due to its large dipole, see Fig. 1) and mainly responsible for the Indole fluorescence spectroscopic behavior.

Even after decades of studies, a clear and complete picture of the photophysics of Indole and Trp in solution is still lacking, with a multitude of mechanisms being proposed over the years [5,20–24]. For Indole, one of the most accepted relaxation schemes involves the transition of the excited Indole from the L_b and L_a states to the dark state, followed by the internal conversion (IC) to the ground eigenstate as occurring through a conical intersection [23,25–28]. Such a scheme is in line with the results of one of our recent works, where we reconstructed the fluorescence-relevant overall relaxation mechanism of the excited Indole in aqueous solution [14] (see Fig. 2), as obtained by using the MD-PMM method [29–32] (Molecular Dynamics - Perturbed Matrix Method) combined with a specific approach for treating the electronic state transitions [14,33,34]. Such a theoretical-computational model allows us to describe the kinetics of relaxation processes even when any reactive event sampling is not accessible. According to our results the first excited eigenstate, initially corresponding to the L_b diabatic state, undergoes a fast interconversion between the L_b and L_a diabatic states (on the time scale of hundreds of fs) followed by a much slower (within the ns time scale) irreversible transition to the diabatic $^1\pi\sigma^*$ state (hereafter referred as the dark state $\pi\sigma^*$) corresponding to the gas phase second electronic excited state at the ground eigenstate geometry.

Among several experimental information available on the emission behavior of aqueous Indole, it has long been observed that its fluorescence quantum yield displays a marked temperature dependence [20–

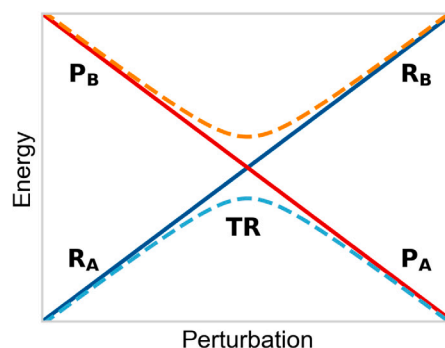


Fig. 3. Schematic description of a single diabatic energy crossing. The reactant R and product P diabatic energy surfaces are represented as solid lines, while the related lower (A) and higher (B) adiabatic energy surfaces are represented as dashed lines. Source: Adapted from Ref. [14].

22,35,36]. This feature, clearly indicating the important temperature effects on the relaxation process, implies a relevant temperature dependence of the radiationless relaxation rates which should be properly reproduced by an accurate theoretical-computational model. Therefore, in this work we use our previously introduced theoretical-computational model to reconstruct the photophysics of the aqueous excited Indole in a wide range of temperatures, accurately reproducing the experimental data reported in the literature and providing a rather detailed characterization of the relaxation mechanism as a function of temperature.

2. Theory

The theory behind the Perturbed Matrix Method (PMM) and Molecular Dynamics-Perturbed Matrix Method (MD-PMM, a QM/MM method [37,38] combining PMM and Molecular Dynamics) can be found in previous works [29–31]. A summary of these approaches, which provided accurate results in the past [14,39–41], as well as the method used to obtain the vibronic absorption and emission spectra [39,42], is presented in Section S1 of the Supplementary Material.

The approach used to model diabatic state transitions was presented in prior studies [14,33,34] and it was applied in this work to model the spectroscopic properties of Indole in aqueous solution at different temperatures. Here we provide an overview of its main concepts and the final equations necessary to calculate all the properties of interest without the lengthy derivations.

2.1. Modeling the singlet electronic excited state transitions

In the present work, we focused on the L_b , $\pi\sigma^*$ and L_a unperturbed electronic eigenstates as the most relevant diabatic electronic states, corresponding to the first three low-lying singlet excited eigenstates of gas-phase Indole calculated at the ground state optimized geometry. Each of these diabatic electronic states is characterized by clearly distinguishable diagonal and transition dipoles, through which we were able to identify the perturbed electronic eigenstates best corresponding to L_b , $\pi\sigma^*$ and L_a in each of the Quantum Center (QC) structure/perturbation conditions we considered, regardless of their energy order.

Considering for a rigid/semirigid QC (such as Indole) two adiabatic energy surfaces A and B (see Fig. 3) involved in the electronic state transition from the reactant (R) diabatic state to the product (P) diabatic state (in this case the L_b , L_a , $\pi\sigma^*$ unperturbed eigenstates), the rate equations for the $R \rightarrow P$ reaction can be derived by taking into account all the reaction steps due to the crossing of the R diabatic vibronic energy surface with all the P vibronic ones involved in each reaction event (see Fig. 4). By assuming that in each reactive trajectory

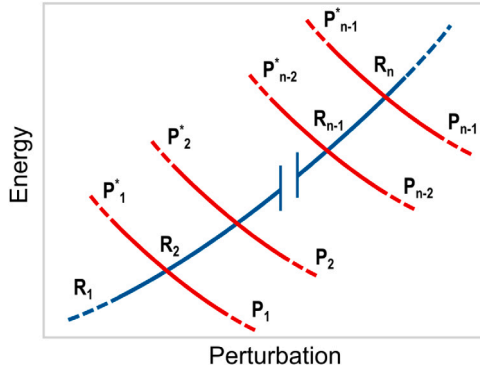


Fig. 4. Schematic representation of the reaction process possibly involving several vibronic state energy crossings defined by the R diabatic vibronic state and the P diabatic vibronic states involved in each reaction event.

Source: Adapted from Ref. [14].

the $R_1 \rightarrow R_n$ reaction steps are completely irreversible with stationary intermediates (irreversible reaction step approximation [33]), and considering the initial reactant condition R_A as the R_1 sub-state of Fig. 4, we obtain [33]

$$[\dot{R}_A] \cong -\alpha_G(2 - \alpha_G)\mathcal{K}_{R_A}[R_A] \quad (1)$$

$$[\dot{P}] \cong -[\dot{R}_A] \cong \alpha_G(2 - \alpha_G)\mathcal{K}_{R_A}[R_A] \quad (2)$$

where α_G is the reaction transmission coefficient [14,33] and \mathcal{K}_{R_A} is the reaction kinetic constant which provide

$$[R_A] \cong [R_A]_0 e^{-\alpha_G(2-\alpha_G)\mathcal{K}_{R_A}t} \quad (3)$$

$$[P] \cong [R_A]_0 \left[1 - e^{-\alpha_G(2-\alpha_G)\mathcal{K}_{R_A}t}\right] \quad (4)$$

with $[R_A]_0$ being the R_A concentration at the beginning of the reaction. It is worth noting that the R and P diabatic electronic energies are provided by the corresponding (perturbed) electronic Hamiltonian matrix diagonal elements (i.e., $[\tilde{H}_e]_{R,R}$ and $[\tilde{H}_e]_{P,P}$, see Section S1 of the Supplementary Material) each calculated at the corresponding unperturbed electronic eigenstate minimum energy geometry [14,33]. From the difference $[\tilde{H}_e]_{P,P} - [\tilde{H}_e]_{R,R}$ we obtain the relevant transition energy of the process and identify the first crossing of the diabatic energies in the R_A trajectories at the first MD frame where such a difference vanishes. Therefore, from the distribution of the time intervals needed to reach the first crossing, evaluating at each crossing the electronic adiabatic fraction χ_e via the Landau-Zener approximation and for each reactive trajectory the squared overlap of the unperturbed vibrational eigenstates involved into the R and P diabatic vibronic states of the subsequent irreversible crossings, we can obtain accurately both \mathcal{K}_{R_A} and α_G [14,33]. However, such a procedure is computationally expensive and not applicable to slow relaxation processes impeding a proper crossing sampling, as occurring for the $L_b \rightarrow \pi\sigma^*$ and $L_a \rightarrow \pi\sigma^*$ transitions characterized by a large mean transition energy. For such a case and more in general to reduce the computational effort needed, we can use specific approximations still providing reasonably accurate α_G and \mathcal{K}_{R_A} estimates. In fact, the reaction transmission coefficient can always be considered in between its lower [14]

$$\alpha_G \approx 1 - (1 - \alpha_e)^{\xi_0^2} \quad (5)$$

and upper

$$\alpha_G \approx 1 - (1 - \alpha_e) = \alpha_e \quad (6)$$

bound approximations, where $\xi_0^2 = |\langle\phi_{R,0}^0|\phi_{P,0}^0\rangle|^2$ is the squared overlap of the R and P unperturbed vibrational ground eigenstates, $\alpha_e = \langle\chi_e\rangle$ is the electronic transmission coefficient as obtained averaging the adiabatic electronic fraction χ_e over all the crossings. Note that the lower bound approximation is accurate when the $R \rightarrow P$ mean transition

energy within the R_A equilibrium ensemble $\langle\Delta U^*\rangle_{R_A} = \langle[\tilde{H}_e]_{P,P} - [\tilde{H}_e]_{R,R}\rangle_{R_A}$ is quite large, with thus most of the R_A reactive trajectories accessing only the first diabatic vibronic energy crossing (i.e., the energy crossing of the R and P diabatic vibronic states involving the unperturbed vibrational ground eigenstates). Differently, the upper bound approximation can be used when the $R \rightarrow P$ mean transition energy within the R_A equilibrium ensemble is small enough to allow each reactive trajectory to access several diabatic energy crossings.

Finally, by using the Landau-Zener approximation we have $\langle\chi_e\rangle \cong 1 - \langle e^{-2\pi|\tilde{H}_{e,R,P}|^2/(\hbar v_{cr})} \rangle$ [14,33] and then within the crossing mean coupling approximation we can write [14]

$$\langle e^{-2\pi|\tilde{H}_{e,R,P}|^2/(\hbar v_{cr})} \rangle \cong e^{-2\pi\langle|\tilde{H}_{e,R,P}|^2\rangle/(\hbar\langle v\rangle_{R_A})} \quad (7)$$

$$\begin{aligned} \langle|\tilde{H}_{e,R,P}|^2\rangle &\cong (\bar{\mu}_{R,P}^0 \cdot \eta_{\parallel})^2 \frac{(\mathcal{U}_{e,P}^0 - \mathcal{U}_{e,R}^0)^2}{|\mu_P^0 - \mu_R^0|^2} + (\bar{\mu}_{R,P}^0 \cdot \eta_{\perp})^2 \langle E_{\perp}^2 \rangle_{R_A} \\ &\quad + 2(\bar{\mu}_{R,P}^0 \cdot \eta_{\parallel})(\bar{\mu}_{R,P}^0 \cdot \eta_{\perp}) \frac{\mathcal{U}_{e,P}^0 - \mathcal{U}_{e,R}^0}{|\mu_P^0 - \mu_R^0|} \langle E_{\perp} \rangle_{R_A} \end{aligned} \quad (8)$$

$$\eta_{\parallel} = \frac{\mu_P^0 - \mu_R^0}{|\mu_P^0 - \mu_R^0|} \quad (9)$$

$$\eta_{\perp} = \frac{\bar{\mu}_{R,P}^0 - \bar{\mu}_{R,P}^0 \cdot \eta_{\parallel}}{|\bar{\mu}_{R,P}^0 - \bar{\mu}_{R,P}^0 \cdot \eta_{\parallel}|} \quad (10)$$

where $\bar{\mu}_{e,R,P}^0$ are obtained from the arithmetic means of each vector component of the R, P diabatic state electronic couplings and of the (unperturbed) electronic transition dipoles as obtained at the R and P energy minima, v_{cr} is the crossing velocity norm, $\langle v \rangle_{R_A}$ is the mean transition energy time derivative v within the R_A equilibrium ensemble, $\mathcal{U}_{e,R}^0$, $\mathcal{U}_{e,P}^0$ and μ_R^0 , μ_P^0 are the unperturbed electronic energies and diagonal electric dipole moments of the reactant and product diabatic states, respectively (each calculated at the corresponding unperturbed eigenstate energy minimum). Moreover, η_{\parallel} and η_{\perp} are the parallel and perpendicular unit vectors to $\mu_P^0 - \mu_R^0$ and $\langle E_{\perp} \rangle_{R_A}$ is the average value of the projection of the perturbing electric field onto η_{\perp} within the R_A equilibrium ensemble.

Similarly, we can evaluate \mathcal{K}_{R_A} without using any crossing sampling by assuming the Gaussian behavior for the fluctuations of the transition energy ΔU^* around its mode value (i.e., the transition energy corresponding to the maximum of the probability distribution) $\Delta U^*_{R_A} \cong \langle\Delta U^*\rangle_{R_A}$, within the R_A transition energy range including $\Delta U^* = 0$ (the first crossing encountered by the R_A trajectories). Finally, considering that within each transition region TR (see Fig. 3) we have a virtually unidirectional flux, we obtain [14,33,34],

$$\mathcal{K}_{R_A} \cong \frac{e^{-\langle\Delta U^*\rangle_{R_A}^2/(2\sigma_{R_A}^2)} \langle v_{cr} \rangle_{TR}}{\sqrt{2\pi\sigma_{R_A}^2}} \quad (11)$$

where $\sigma_{R_A}^2$ is the variance of the transition energy within the R_A equilibrium ensemble and $\langle v_{cr} \rangle_{TR}$ is the equilibrium average of the norm of the crossing velocity v_{cr} . $\langle v_{cr} \rangle_{TR}$ can be approximated to the average of the norm of the transition energy time derivative v within the R_A equilibrium ensemble (i.e., $\langle v_{cr} \rangle_{TR} \cong \langle v \rangle_{R_A}$). In this paper we always use the Gaussian and crossing mean coupling approximations to obtain the kinetic constants and transmission coefficients of interest.

3. Computational details

3.1. QM calculations

The structures corresponding to the energy minima of the unperturbed electronic ground state, L_b , L_a , and $\pi\sigma^*$ excited states of Indole were obtained using Coupled Cluster Singles and Doubles (CCSD) and Equation-of-Motion-Coupled Cluster Singles and Doubles (EOM-CCSD) with 6-311+G(d) as the basis set. These structures were used as the

reference QC geometries for the Molecular Dynamics-Perturbed Matrix Method (MD-PM) calculations. It should be noted that while for the ground, L_b and L_a states the optimization was carried out considering Indole in the gas phase, we could not reach convergence in the same condition for the $\pi\sigma^*$ state. This difficulty possibly arises from the shallowness of the minimum of this state [23]. Therefore, to obtain the convergence in this calculation, Indole was considered in aqueous solution for the optimization only (using integral equation formalism of the polarizable continuum model, IEFPCM, as the model [43]). The in vacuo electronic properties of the ground state and first six low-lying singlet excited states at each of the obtained reference geometries were calculated using CCSD and EOM-CCSD with 6-311+G(d) as the basis set. The vibrational eigenstates corresponding to the L_b , L_a , and $\pi\sigma^*$ excited states were obtained using Time-Dependent Density Functional Theory (TD-DFT), with M06-2X [44] as the functional and 6-311+G(d) as the basis set. The vibronic transitions between these states were calculated using an approach we described in a recent paper [39]. Such a choice was motivated by the high computational cost that a full EOM-CCSD treatment would require and was justified in our previous works [14,39].

Finally, the unperturbed (i.e., in vacuo) energies of the L_b and L_a were corrected to match the calculated 0-0 vibronic transition to the experimental (gas phase) values [45], when the $L_b \rightleftharpoons L_a$ reactions was considered. These shifts are -0.32 eV for $GS \rightarrow L_b$ and -0.57 eV for $GS \rightarrow L_a$. It is worth noting that no such corrections to L_b and L_a were applied when dealing with transitions involving $\pi\sigma^*$, since the experimental data for the dark states are not obtainable.

The geometry optimizations and the calculation of the vibrational eigenstates were performed using Gaussian 16 [46], while the electronic properties were obtained using both QChem 5.3 [47] and Gaussian 16 [46] (to obtain the ESP charges [48,49]).

3.2. MD simulations

An equilibrium NVT MD simulation of 80 ns, with a timestep of 2 fs, was performed for each of the values of temperatures (278, 290, 300, 310, 323, 340, 360 K) and for each Indole electronic state (GS, L_b and L_a), for a system consisting of an Indole molecule in a cubic box containing 1276 CHARMM-modified TIP3P water molecules [50,51]. The size of the box (of side around 3.4 nm) was modified for each considered system (i.e., for each value of temperature and for each diabatic state we adjusted the size of the box) in order to reproduce the experimental condition of isobaric insertion of the solute in liquid water at infinite dilution [52]. Periodic boundary conditions were used, as well as the velocity rescaling thermostat to achieve the canonical sampling [53]. The particle mesh Ewald method was used to treat the long-range electrostatic interactions [54]. All bonds were frozen using the LINCS algorithm [55].

Moreover, non-equilibrium simulations of 50 ps with a reduced timestep of 1 fs were carried out in order to estimate the transition energy time derivative \dot{v} with higher accuracy (see Theory section), in the same conditions as the equilibrium ones, for each of the systems.

The forcefield used was CHARMM36 [56,57]. For the simulations in the excited state, the atomic charges in the forcefield were replaced with the ESP charges corresponding to that state calculated at the QM level, while leaving the other (ground state) parameters intact. This was justified by the rigidity of the structure of Indole, which does not undergo significant deformation even after excitation, as the QM calculations show (see Table S1 in the Supplementary Material). Such an approach proved to be a reasonable approximation in our previous work [14,58–60]. On the other hand, when treating a flexible system, a reparametrization of the classical force field would be required. All the MD simulations were performed using the Gromacs 2020.1 software package [61].

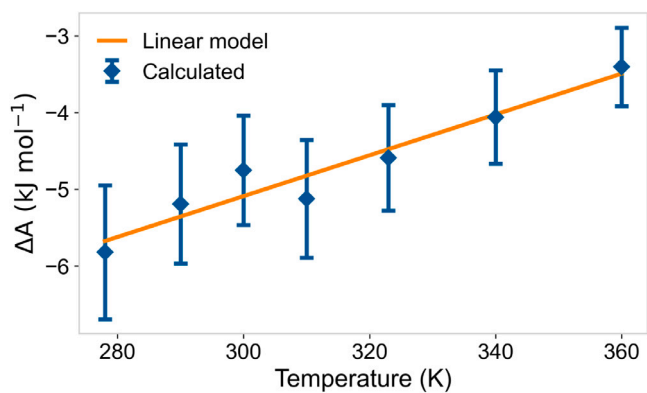


Fig. 5. Free energy change ΔA for the $L_b \rightarrow L_a$ transition calculated at different temperatures (blue, with the error bars corresponding to \pm a standard error). The linear fitting is shown in orange.

3.3. MD-PM simulations

The MD-PM calculations using the atom-based approximation [31] (see Theory section) were performed using 40,000 frames extracted from the equilibrium MD simulations (i.e., only one every 1000 timesteps has been used) and 50,000 frames from the non-equilibrium MD simulations for every value of temperature considered. The MD-PM simulations were carried out using the PyPM program [32].

4. Results and discussion

As established by previous results [14], and supported by other experimental and theoretical studies [62,63], at room temperature we expect a fast interconversion (hundreds of fs timescale) between the two diabatic states (L_b and L_a) corresponding to the first excited state condition after the absorption of the photon, with much slower subsequent transitions to the dark state (i.e., $L_b \rightarrow \pi\sigma^*$ and $L_a \rightarrow \pi\sigma^*$). Therefore, we assumed the equilibrium mixture of the L_b and L_a diabatic state populations as present during the whole relaxation process of the first excited state as obtained by fluorescence data. The same assumption can be considered valid between 278 and 360 K, as shown by the calculated reaction mean lifetimes (see Tables 1 and 4).

At 300 K, the equilibrium population fractions were determined to be 0.13 for L_b and 0.87 for L_a [14]. The calculations carried out in this work confirm that, despite the L_b relative stability increase due to the rise of temperature, the L_a diabatic state remains thermodynamically much more stable in the whole range of temperature considered, as shown in Table 2. The reported Helmholtz free energy variations ΔA associated to the $L_b \rightarrow L_a$ transition were calculated using:

$$\Delta A = (k_B T / 2) \ln \{ \langle e^{\Delta U' / (k_B T)} \rangle_{L_a} / \langle e^{-\Delta U' / (k_B T)} \rangle_{L_b} \} \quad (12)$$

where $\langle \dots \rangle_{L_a/L_b}$ refers to averaging over the L_a/L_b ensembles and $\Delta U'$ indicates the transition energy associated to $L_b \rightarrow L_a$.

The equilibrium population fractions of L_b and L_a , referred as f_b and f_a respectively, were obtained by:

$$f_a = \frac{K_{eq}}{1 + K_{eq}} \quad (13)$$

$$f_b = \frac{1}{1 + K_{eq}} \quad (14)$$

$$K_{eq} = \frac{f_a}{f_b} = e^{-\Delta A / (k_B T)} \quad (15)$$

where K_{eq} is the equilibrium constant for the $L_b \rightleftharpoons L_a$ reaction.

By using a linear model to fit the predicted ΔA (see Fig. 5) we obtain the values of the internal energy change $\Delta U = -13$ kJ mol⁻¹ and entropy change $\Delta S = -2.7 \cdot 10^{-2}$ kJ mol⁻¹ K⁻¹ for the $L_b \rightarrow L_a$ transition.

Table 1

Mean transition energy $\langle \Delta U \rangle_{R_A}$, standard deviation of the transition energy σ_{R_A} , mean crossing velocity norm as provided by the R_A mean transition energy time derivative norm $\langle \dot{v} \rangle_{R_A}$, fully adiabatic transition mean lifetime $\tau_0 = 1/\mathcal{K}_{R_A}$, transmission coefficient α_G and the reaction mean lifetime τ for the $L_b \rightarrow L_a$ and $L_a \rightarrow L_b$ transitions. We calculated α_G and related τ values using either $\alpha_G \approx 1 - (1 - \alpha_e)^{S_0}$ or $\alpha_G \approx 1 - (1 - \alpha_e)$ (the latter shown between parenthesis). We estimate a relative standard error of 1.4% and 0.4% for $\langle \Delta U \rangle_{R_A}$ and a relative standard error of 1% and 1.8% for τ_0 for the $L_b \rightarrow L_a$ and $L_a \rightarrow L_b$ reactions respectively.

T (K)	$\langle \Delta U \rangle_{R_A}$ (kJ mol ⁻¹)	σ_{R_A} (kJ mol ⁻¹)	$\langle \dot{v}_{cr} \rangle_{R_A}$ (kJ mol ⁻¹ fs ⁻¹)	τ_0 (fs)	α_G	τ (fs)
$L_b \rightarrow L_a$						
278	3.20	7.04	0.38	102	0.86 (1)	104 (102)
290	3.42	7.02	0.39	102	0.86 (1)	104 (102)
300	3.62	7.09	0.39	104	0.86 (1)	106 (104)
310	3.76	7.04	0.39	104	0.86 (1)	106 (104)
323	4.07	7.10	0.39	108	0.86 (1)	110 (108)
340	4.34	7.21	0.40	108	0.85 (1)	111 (108)
360	4.54	7.19	0.40	110	0.85 (1)	112 (110)
$L_a \rightarrow L_b$						
278	13.91	6.33	0.40	887	0.85 (1)	906 (887)
290	13.51	6.43	0.39	753	0.86 (1)	769 (753)
300	13.15	6.54	0.40	613	0.85 (1)	627 (613)
310	12.85	6.55	0.41	547	0.85 (1)	560 (547)
323	12.46	6.64	0.41	474	0.85 (1)	485 (474)
340	11.89	6.76	0.41	388	0.85 (1)	397 (388)
360	11.13	6.85	0.41	315	0.85 (1)	322 (315)

Table 2

Free energy change ΔA for the $L_b \rightarrow L_a$ transition (with ΔU being the $L_b \rightarrow L_a$ transition energy), the equilibrium constant $K_{eq} = f_a/f_b$, and the L_b and L_a state equilibrium fractions f_b and f_a . We estimate a relative standard error of 10% for the values of ΔA .

T (K)	ΔA (kJ mol ⁻¹)	K_{eq}	f_b	f_a
278	-5.82	12.39	0.07	0.93
290	-5.19	8.61	0.10	0.90
300	-4.75	6.72	0.13	0.87
310	-5.12	7.29	0.12	0.88
323	-4.59	5.52	0.15	0.85
340	-4.06	4.20	0.19	0.81
360	-3.40	3.12	0.24	0.76

From the L_b and L_a states, Indole can either emit or irreversibly transit to $\pi\sigma^*$, where it non-radiatively relaxes to the ground eigenstate [14,23]. The mean lifetimes corresponding to both of these processes were estimated and reported in Tables 3 and 4.

Fig. 7 shows the predicted equilibrium emission spectra, obtained as the sum of the contributions arising from the L_b and L_a states, weighted by the corresponding equilibrium population fractions f_b and f_a . These results are in agreement with the experimental findings of Kirby et al. [20] and Klein et al. [36], both reporting the absence of any relevant change in the measured emission maximum wavelength and broadening due to the increasing temperature, consistently with our result of the first excited state largely corresponding to the L_a diabatic state at all temperatures (see Table 2). It should be noted that the slight variations due to the temperature increase observed in our calculated emission spectra (in particular concerning the tiny high energy peak corresponding to the L_b population, see Fig. 6) might arise from the diabatic state approximation used to model the perturbed electronic first excited eigenstate, possibly resulting in an overestimated L_b spectral signal.

Finally, the overall mean radiative τ_r and radiationless τ_{nr} relaxation mean lifetimes from the equilibrium mixture of L_b and L_a (Table 3 and Fig. 9), to be compared to the experimental fluorescence data, can be approximated considering only the L_b and L_a radiative relaxation to the ground eigenstate and radiationless transitions to the dark state, as the other radiationless relaxation processes possibly occurring are much slower and thus can be disregarded [22,64,65]. Therefore, we obtained the fluorescence quantum yield

$$Q = \frac{\tau_r^{-1}}{\tau_{nr}^{-1} + \tau_r^{-1}} \quad (16)$$

Table 3

Calculated radiative relaxation mean lifetimes for the $L_b \xrightarrow{-h\nu} GS$ ($\tau_{r,b}$) and the $L_a \xrightarrow{-h\nu} GS$ ($\tau_{r,a}$) emissions and for the emission of the first excited state as the equilibrium mixture of L_b and L_a $\tau_r = (f_b/\tau_{r,b} + f_a/\tau_{r,a})^{-1}$ at different values of temperature (the unreported noise is below 0.1 ns).

T (K)	$\tau_{r,b}$ (ns)	$\tau_{r,a}$ (ns)	τ_r (ns)
278	56.1	20.1	21.1
290	56.0	20.1	21.5
300	56.0	20.0	21.8
310	55.9	20.0	21.7
323	55.8	20.0	22.2
340	55.8	19.9	22.7
360	55.7	19.9	23.5

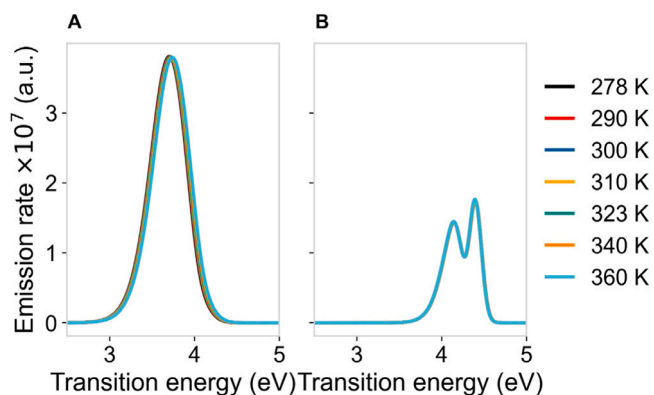


Fig. 6. Calculated emission spectra corresponding to (A) $L_a \xrightarrow{-h\nu} GS$ and (B) $L_b \xrightarrow{-h\nu} GS$ of indole in aqueous solution at different temperatures.

by using

$$\tau_r \cong (f_b/\tau_{r,b} + f_a/\tau_{r,a})^{-1} \quad (17)$$

$$\tau_{nr} \cong (f_b/\tau_{nr,b} + f_a/\tau_{nr,a})^{-1} \quad (18)$$

where $\tau_{r,b}$, $\tau_{r,a}$ and $\tau_{nr,b}$, $\tau_{nr,a}$ are the radiative and radiationless mean lifetimes of the L_b and L_a populations, respectively, with the former as obtained by the emission spectra and the latter provided by the rate constants for the $L_b \rightarrow \pi\sigma^*$ and $L_a \rightarrow \pi\sigma^*$ transitions.

It is worth noting that there are discrepancies in the experimental data reported in the literature (see Fig. 8). Among the four works

Table 4

Mean transition energy $\langle \Delta U \rangle_{R_A}$, standard deviation of the transition energy σ_{R_A} , mean crossing velocity norm as provided by the R_A mean transition energy time derivative norm $\langle v \rangle_{R_A}$, fully adiabatic transition mean lifetime $\tau_0 = 1/\mathcal{K}_{R_A}$, transmission coefficient α_G and the reaction mean lifetime τ for the $L_b \rightarrow \pi\sigma^*$ and $L_a \rightarrow \pi\sigma^*$ transitions. We calculated α_G and related τ values using $\alpha_G \approx 1 - (1 - \alpha_e)^{\frac{1}{2}}$. We estimate a relative standard error of 0.20% and 0.18% for $\langle \Delta U \rangle_{R_A}$ and a relative standard error of 4.6% and 10.0% for τ_0 for the $L_b \rightarrow \pi\sigma^*$ and $L_a \rightarrow \pi\sigma^*$ reactions respectively.

T (K)	$\langle \Delta U \rangle_{R_A}$ (kJ mol ⁻¹)	σ_{R_A} (kJ mol ⁻¹)	$\langle v \rangle_{R_A}$ (kJ mol ⁻¹ fs ⁻¹)	τ_0 (ps)	α_G	τ (ns)
$L_b \rightarrow \pi\sigma^*$						
278	128.57	29.97	1.68	892	0.02	21.9
290	127.57	30.45	1.71	580	0.02	14.3
300	127.35	30.91	1.66	453	0.02	10.8
310	126.94	31.03	1.70	393	0.02	9.44
323	125.91	31.28	1.74	299	0.02	7.32
340	124.78	31.70	1.79	205	0.02	5.15
360	123.10	32.49	1.76	121	0.02	2.92
$L_a \rightarrow \pi\sigma^*$						
278	139.57	32.24	1.93	985	0.06	8.14
290	138.53	32.77	1.97	633	0.06	5.09
300	138.20	33.16	1.97	498	0.07	3.98
310	137.27	33.13	2.01	442	0.06	3.54
323	136.38	33.70	1.98	307	0.07	2.38
340	134.68	34.40	2.02	183	0.07	1.38
360	132.79	35.08	2.03	112	0.07	0.84

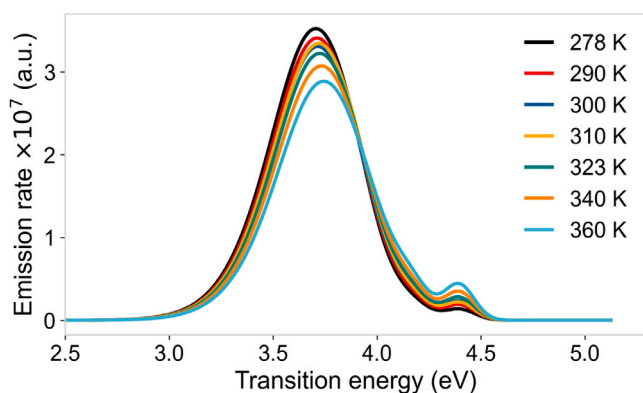


Fig. 7. Calculated emission spectra of Indole in aqueous solution at different values of temperature.

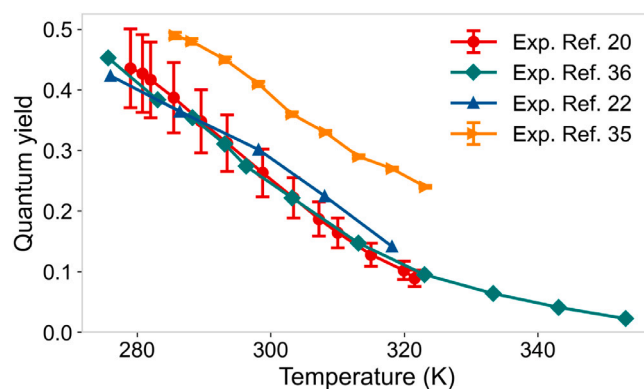


Fig. 8. Experimental fluorescence quantum yield of indole in aqueous solution measured at different temperatures taken from the literature [20,22,35,36]. The error was shown only when reported by the original authors.

we found [20,22,35,36], only three of them present similar experimental results [20,22,36]. After discarding the seeming outlier [35], we decided to compare our computational results with the values measured by Kirby et al. [20] when possible (it is the only paper also reporting the standard error), while using the measured data from Klein et al. [36] in the higher temperature range neglected by Kirby et al. In order to obtain the values of the experimental τ_{nr} from the reported experimental values of Q (see Fig. 9), we used $\tau_{nr} = \tau_r / (Q^{-1} - 1)$ with the experimental $\tau_r = 14.29$ ns as reported by Kirby et al. (from the same paper we collected the experimental Q between 278.15 and 323.15 K). We assumed such an experimental τ_r to be a reasonable value to be used also when considering the quantum yield data as obtained by Klein et al. as the quantum yields reported in such experimental works for the shared temperature range are very similar (see Fig. 6). Finally, the experimental τ_r was considered constant for the whole range of temperature considered, an approximation supported by both our calculations (see Table 3) and the literature data [20,36].

In Figs. 9 and 10 we compare our estimated τ_{nr} and Q with the corresponding experimental values. From these figures it is evident the accuracy, within the noise, of the calculated radiationless relaxation mean lifetime and quantum yield in reproducing the corresponding experimental properties within the whole temperature range considered.

5. Conclusions

By means of the MD-PMM approach and the Gaussian and crossing mean coupling approximations, we reconstructed the temperature dependence of the fluorescence properties of aqueous Indole by modeling the (perturbed) electronic first excited eigenstate transitions in terms of the interconversions of the L_b , L_a and $\pi\sigma^*$ diabatic states. The results obtained confirmed the validity of the relaxation scheme we proposed in a previous paper [14], indicating the transition from the equilibrium mixture of the L_b and L_a diabatic states to the dark (diabatic) state $\pi\sigma^*$ as the main process involved in the relaxation of aqueous Indole first electronic excited eigenstate as detected by fluorescence experiments. Such an electronic state transition rate increases at higher temperatures where the transition energy fluctuations become larger due to the increased solvent fluctuations. Although we used the diabatic state approximation for treating the perturbed electronic first excited eigenstate (i.e., we neglect any diabatic state mixing in the excited eigenstate wavefunction) possibly providing some inaccuracies (e.g., the intensities of the emission spectra), the excellent results obtained over a wide range of temperatures for a system as challenging as aqueous Indole, further show the accuracy and robustness of the theoretical-computational model employed. Because of its low computational cost, such an approach is able to provide quantitative predictions even for processes that are too slow and complex to be addressed by more conventional (but more resource-demanding) methods [63,66–68]. Finally,

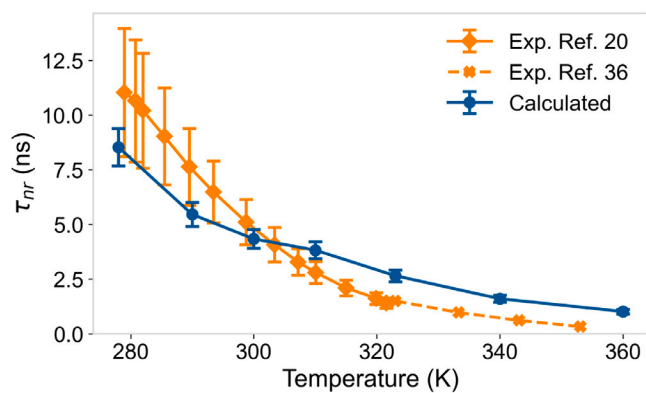


Fig. 9. Calculated (blue) and experimental (orange) lifetime of the non-radiative relaxation processes as a function of temperature (the error bars correspond to \pm a standard error). The experimental data were obtained from $\tau_{nr} = \tau_r / (Q^{-1} - 1)$ using the values of Q obtained by Kirby et al. [20] in the range between 278.15 and 323.15 K (where the authors report the standard error on their measurements) and by Klein et al. [36] between 323.15 and 353.15 K (i.e., outside the temperature range considered by Kirby et al.; the authors do not provide experimental error estimates). It is worth noting that at the temperatures where data from both works are available, such measurements are very close to each other (see Fig. 6). For τ_r , we considered the value measured by Kirby et al. [20].

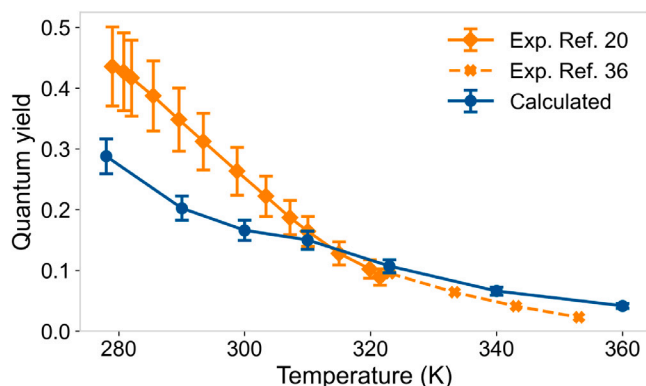


Fig. 10. Calculated (blue) and measured [20,36] (orange, see caption in Fig. 9) fluorescence quantum yield as a function of temperature (the error bars correspond to \pm a standard error).

the results obtained in this paper suggest that additional computational studies using different solvents can be performed using the proposed approach to further understand the environmental effects on the fluorescence properties of Indole [5,20,69,70].

CRediT authorship contribution statement

Cheng Giuseppe Chen: Validation, Investigation, Formal analysis, Data curation. **Andrea Amadei:** Writing – review & editing, Writing – original draft, Methodology, Conceptualization. **Marco D'Abramo:** Writing – review & editing, Writing – original draft, Validation, Supervision, Project administration, Conceptualization.

Declaration of competing interest

The authors declare that they have no known competing financial interests or personal relationships that could have appeared to influence the work reported in this paper.

Data availability

Data will be made available on request.

Appendix A. Supplementary data

Supplementary material related to this article can be found online at <https://doi.org/10.1016/j.saa.2024.124096>.

References

- [1] Y. Chen, B. Liu, H.-T. Yu, M.D. Barkley, The peptide bond quenches indole fluorescence, *J. Am. Chem. Soc.* 118 (39) (1996) 9271–9278, <http://dx.doi.org/10.1021/ja961307u>.
- [2] A. Peralta Conde, V. Ovejias, R. Montero, F. Castaño, A. Longarte, Influence of solvation on the indole photophysics: Ultrafast dynamics of indole–water clusters, *Chem. Phys. Lett.* 530 (2012) 25–30, <http://dx.doi.org/10.1016/j.cplett.2012.01.060>.
- [3] A. Iqbal, V.G. Stavros, Exploring the time scales of H-atom elimination from photoexcited indole, *J. Phys. Chem. A* 114 (1) (2010) 68–72, <http://dx.doi.org/10.1021/jp908195k>, PMID: 19928773.
- [4] R. Montero, A.P. Conde, V. Ovejias, F. Castaño, A. Longarte, Ultrafast photophysics of the isolated indole molecule, *J. Phys. Chem. A* 116 (11) (2012) 2698–2703, <http://dx.doi.org/10.1021/jp207750y>, PMID: 22050115.
- [5] J. Albani, Origin of tryptophan fluorescence lifetimes. Part 2: Fluorescence lifetimes origin of tryptophan in proteins, *J. Fluoresc.* 24 (1) (2014) 105–117, <http://dx.doi.org/10.1007/s10895-013-1274-y>.
- [6] M.R. Hilaire, D. Mukherjee, T. Troxler, F. Gai, Solvent dependence of cyanoindole fluorescence lifetime, *Chem. Phys. Lett.* 685 (2017) 133–138, <http://dx.doi.org/10.1016/j.cplett.2017.07.038>.
- [7] L. Serrano-Andrés, A.C. Borin, A theoretical study of the emission spectra of indole and its analogs: indene, benzimidazole, and 7-azaindole, *Chem. Phys.* 262 (2000) 267–283, [http://dx.doi.org/10.1016/S0301-0104\(00\)00335-9](http://dx.doi.org/10.1016/S0301-0104(00)00335-9).
- [8] C. Brand, J. Küpper, D.W. Pratt, W.L. Meerts, D. Krügler, J. Tatchen, M. Schmitt, Vibronic coupling in indole: I. Theoretical description of the 1La–1Lb interaction and the electronic spectrum, *Phys. Chem. Chem. Phys.* 12 (2010) 4968–4979, <http://dx.doi.org/10.1039/C001776K>.
- [9] A. Giussani, M. Merchán, D. Roca-Sanjuán, R. Lindh, Essential on the photophysics and photochemistry of the indole chromophore by using a totally unconstrained theoretical approach, *J. Chem. Theory Comput.* 7 (12) (2011) 4088–4096, <http://dx.doi.org/10.1021/ct200646r>, PMID: 26598354.
- [10] D. Brisker-Klaiman, A. Dreuw, Explaining level inversion of the 1a and 1b states of indole and indole derivatives in polar solvents, *ChemPhysChem* 16 (2015) 1695–1702, <http://dx.doi.org/10.1002/CPHC.201500073>.
- [11] R. Omidyan, M. Omidyan, A. Mohammadzadeh, Electronically excited state of neutral/protonated, indole/5-hydroxyindole–water clusters: A theoretical study, *RSC Adv.* 6 (2016) 33148–33158, <http://dx.doi.org/10.1039/C6RA06716F>.
- [12] S. Abou-Hatab, S. Matsika, Theoretical investigation of positional substitution and solvent effects on n-cyanoindole fluorescent probes, *J. Phys. Chem. B* 123 (34) (2019) 7424–7435, <http://dx.doi.org/10.1021/acs.jpcc.9b05961>, PMID: 31373821.
- [13] G. Díaz Mirón, M.C. González Lebrero, Fluorescence quantum yields in complex environments from QM-MM TDDFT simulations: The case of indole in different solvents, *J. Phys. Chem. A* 124 (46) (2020) 9503–9512, <http://dx.doi.org/10.1021/acs.jpca.0c06631>, PMID: 33166141.
- [14] C.G. Chen, M. Giustini, M. D'Abramo, A. Amadei, Unveiling the excited state dynamics of indole in solution, *J. Chem. Theory Comput.* 19 (13) (2023) 4114–4124, <http://dx.doi.org/10.1021/acs.jctc.3c00221>, PMID: 37329333.
- [15] J.T. Vivian, P.R. Callis, Mechanisms of tryptophan fluorescence shifts in proteins, *Biophys. J.* 80 (5) (2001) 2093–2109, [http://dx.doi.org/10.1016/S0006-3495\(01\)76183-8](http://dx.doi.org/10.1016/S0006-3495(01)76183-8).
- [16] J. Włodarczyk, B. Kierdaszuk, Interpretation of fluorescence decays using a power-like model, *Biophys. J.* 85 (1) (2003) 589–598.
- [17] P.R. Callis, T. Liu, Quantitative prediction of fluorescence quantum yields for tryptophan in proteins, *J. Phys. Chem. B* 108 (14) (2004) 4248–4259, <http://dx.doi.org/10.1021/jp0310551>.
- [18] S. Enoki, K. Saeki, K. Maki, K. Kuwajima, Acid denaturation and refolding of green fluorescent protein, *Biochem.* 43 (44) (2004) 14238–14248, <http://dx.doi.org/10.1021/bi048733+>, PMID: 15518574.
- [19] P. Sindrewicz, X. Li, E.A. Yates, J.E. Turnbull, L.-Y. Lian, L.-G. Yu, Intrinsic tryptophan fluorescence spectroscopy reliably determines galectin–ligand interactions, *Sci. Rep.* 9 (1) (2019) <http://dx.doi.org/10.1038/s41598-019-47658-8>.
- [20] E.P. Kirby, R.F. Steiner, Influence of solvent and temperature upon the fluorescence of indole derivatives, *J. Phys. Chem.* 74 (26) (1970) 4480–4490, <http://dx.doi.org/10.1021/j100720a004>.
- [21] J. Eisinger, G. Navon, Fluorescence Quenching and Isotope Effect of Tryptophan, *J. Chem. Phys.* 50 (5) (1969) 2069–2077, <http://dx.doi.org/10.1063/1.1671335>.
- [22] J. Feitelson, The formation of hydrated electrons from the excited state of indole derivatives, *Photochem. Photobiol.* 13 (2) (1971) 87–96, <http://dx.doi.org/10.1111/j.1751-1097.1971.tb06095.x>.
- [23] A.L. Sobolewski, W. Domcke, C. Dedonder-Lardeux, C. Jouvet, Excited-state hydrogen detachment and hydrogen transfer driven by repulsive $^1\pi\sigma^*$ states: A new paradigm for nonradiative decay in aromatic biomolecules, *Phys. Chem. Chem. Phys.* 4 (2002) 1093–1100, <http://dx.doi.org/10.1039/B110941N>.

- [24] A. Szabo, D. Rayner, Fluorescence decay of tryptophan conformers in aqueous solution, *J. Am. Chem. Soc.* 102 (2) (1980) 554–563.
- [25] A.L. Sobolewski, W. Domcke, Ab initio investigations on the photophysics of indole, *Chem. Phys. Lett.* 315 (3) (1999) 293–298, [http://dx.doi.org/10.1016/S0009-2614\(99\)01249-X](http://dx.doi.org/10.1016/S0009-2614(99)01249-X).
- [26] B.C. Dian, A. Longarte, T.S. Zwier, Hydride stretch infrared spectra in the excited electronic states of indole and its derivatives: Direct evidence for the $^1\pi\sigma^*$ state, *J. Chem. Phys.* 118 (6) (2003) 2696–2706, <http://dx.doi.org/10.1063/1.1536616>.
- [27] C. Dedonder-Lardeux, C. Jouvett, S. Perun, A.L. Sobolewski, External electric field effect on the lowest excited states of indole: ab initio and molecular dynamics study, *Phys. Chem. Chem. Phys.* 5 (2003) 5118–5126, <http://dx.doi.org/10.1039/B308866A>.
- [28] S. Soorkia, C. Jouvett, G. Grégoire, UV photoinduced dynamics of conformer-resolved aromatic peptides, *Chem. Rev.* 120 (7) (2020) 3296–3327, <http://dx.doi.org/10.1021/acs.chemrev.9b00316>, PMID: 31424927.
- [29] M. Aschi, R. Spezia, A. Di Nola, A. Amadei, A first-principles method to model perturbed electronic wavefunctions: the effect of an external homogeneous electric field, *Chem. Phys. Lett.* 344 (3) (2001) 374–380, [http://dx.doi.org/10.1016/S0009-2614\(01\)00638-8](http://dx.doi.org/10.1016/S0009-2614(01)00638-8).
- [30] A. Amadei, M. D'Alessandro, M. D'Abramo, M. Aschi, Theoretical characterization of electronic states in interacting chemical systems, *J. Chem. Phys.* 130 (8) (2009) 084109, <http://dx.doi.org/10.1063/1.3080887>.
- [31] L. Zanetti-Polzi, S. Del Gaudio, I. Daidone, M. D'Abramo, V. Barone, M. Aschi, A. Amadei, Extending the perturbed matrix method beyond the dipolar approximation: comparison of different levels of theory, *Phys. Chem. Chem. Phys.* 20 (2018) 24369–24378, <http://dx.doi.org/10.1039/C8CP04190C>.
- [32] C.G. Chen, A.N. Nardi, A. Amadei, M. D'Abramo, PyMM: An open-source python program for QM/MM simulations based on the perturbed matrix method, *J. Chem. Theory Comput.* 19 (1) (2023) 33–41, <http://dx.doi.org/10.1021/acs.jctc.2c00767>, PMID: 36378163.
- [33] A. Amadei, M. Aschi, Theoretical-computational modeling of charge transfer and intersystem crossing reactions in complex chemical systems, *RSC Adv.* 8 (2018) 27900–27918, <http://dx.doi.org/10.1039/C8RA03900C>.
- [34] A.N. Nardi, M. D'Abramo, A. Amadei, Modeling charge transfer reactions by hopping between electronic ground state minima: Application to hole transfer between DNA bases, *Molecules* 27 (21) (2022) <http://dx.doi.org/10.3390/molecules27217408>.
- [35] M.S. Walker, T.W. Bednar, R. Lumry, F. Humphries, Exciplex studies-iv. Radiative and non-radiative relaxation of the fluorescent state of indole⁺, *Photochem. Photobiol.* 14 (2) (1971) 147–161, <http://dx.doi.org/10.1111/j.1751-1097.1971.tb06159.x>.
- [36] R. Klein, I. Tatischeff, Temperature fluorescence quenching of indole and water structure, *Chem. Phys. Lett.* 51 (2) (1977) 333–338, [http://dx.doi.org/10.1016/0009-2614\(77\)80415-6](http://dx.doi.org/10.1016/0009-2614(77)80415-6).
- [37] H. Lin, D.G. Truhlar, QM/MM: what have we learned, where are we, and where do we go from here? *Theor. Chem. Acc.* 117 (2007) 185–199.
- [38] H.M. Senn, W. Thiel, QM/MM methods for biomolecular systems, *Angew. Chem. Int. Edn* 48 (7) (2009) 1198–1229, <http://dx.doi.org/10.1002/anie.200802019>.
- [39] C.G. Chen, M. Aschi, M. D'Abramo, A. Amadei, A simplified treatment for efficiently modeling the spectral signal of vibronic transitions: Application to aqueous indole, *Molecules* 27 (23) (2022) <http://dx.doi.org/10.3390/molecules27238135>.
- [40] V. D'Annibale, A.N. Nardi, A. Amadei, M. D'Abramo, Theoretical characterization of the reduction potentials of nucleic acids in solution, *J. Chem. Theory Comput.* 17 (3) (2021) 1301–1307, <http://dx.doi.org/10.1021/acs.jctc.0c00728>, PMID: 33621084.
- [41] M.L. De Sciscio, V. D'Annibale, M. D'Abramo, Theoretical evaluation of sulfur-based reactions as a model for biological antioxidant defense, *Int. J. Mol. Sci.* 23 (23) (2022) 14515.
- [42] M. D'Abramo, M. Aschi, A. Amadei, Theoretical modeling of UV-Vis absorption and emission spectra in liquid state systems including vibrational and conformational effects: Explicit treatment of the vibronic transitions, *J. Chem. Phys.* 140 (16) (2014) 164104, <http://dx.doi.org/10.1063/1.4871626>.
- [43] G. Scalmani, M.J. Frisch, Continuous surface charge polarizable continuum models of solvation. I. General formalism, *J. Chem. Phys.* 132 (11) (2010) 114110, <http://dx.doi.org/10.1063/1.3359469>.
- [44] Y. Zhao, D.G. Truhlar, The M06 suite of density functionals for main group thermochemistry, thermochemical kinetics, noncovalent interactions, excited states, and transition elements: two new functionals and systematic testing of four M06-class functionals and 12 other functionals, *Theor. Chem. Acc.* 120 (1) (2008) 215–241, <http://dx.doi.org/10.1007/s00214-007-0310-x>.
- [45] L. Serrano-Andrés, B.O. Roos, Theoretical study of the absorption and emission spectra of indole in the gas phase and in a solvent, *J. Am. Chem. Soc.* 118 (1) (1996) 185–195, <http://dx.doi.org/10.1021/ja952035i>.
- [46] M.J. Frisch, G.W. Trucks, H.B. Schlegel, G.E. Scuseria, M.A. Robb, J.R. Cheeseman, G. Scalmani, V. Barone, G.A. Petersson, H. Nakatsuji, X. Li, M. Caricato, A.V. Marenich, J. Bloino, B.G. Janesko, R. Gomperts, B. Mennucci, H.P. Hratchian, J.V. Ortiz, A.F. Izmaylov, J.L. Sonnenberg, D. Williams-Young, F. Ding, F. Lipparini, F. Egidi, J. Goings, B. Peng, A. Petrone, T. Henderson, D. Ranasinghe, V.G. Zakrzewski, J. Gao, N. Rega, G. Zheng, W. Liang, M. Hada, M. Ehara, K. Toyota, R. Fukuda, J. Hasegawa, M. Ishida, T. Nakajima, Y. Honda, O. Kitao, H. Nakai, T. Vreven, K. Throssell, J.A. Montgomery, Jr., J.E. Peralta, F. Ogliaro, M.J. Bearpark, J.J. Heyd, E.N. Brothers, K.N. Kudin, V.N. Staroverov, T.A. Keith, R. Kobayashi, J. Normand, K. Raghavachari, A.P. Rendell, J.C. Burant, S.S. Iyengar, J. Tomasi, M. Cossi, J.M. Millam, M. Klene, C. Adamo, R. Cammi, J.W. Ochterski, R.L. Martin, K. Morokuma, O. Farkas, J.B. Foresman, D.J. Fox, Gaussian 16 Revision B.01, Gaussian Inc., Wallingford CT, 2016.
- [47] Y. Shao, Z. Gan, E. Epifanovsky, A.T. Gilbert, M. Wormit, J. Kussmann, A.W. Lange, A. Behn, J. Deng, X. Feng, et al., Advances in molecular quantum chemistry contained in the Q-chem 4 program package, *Mol. Phys.* 113 (2) (2015) 184–215.
- [48] U.C. Singh, P.A. Kollman, An approach to computing electrostatic charges for molecules, *J. Comput. Chem.* 5 (2) (1984) 129–145, <http://dx.doi.org/10.1002/jcc.540050204>.
- [49] B.H. Besler, K.M. Merz, Jr., P.A. Kollman, Atomic charges derived from semiempirical methods, *J. Comput. Chem.* 11 (4) (1990) 431–439, <http://dx.doi.org/10.1002/jcc.540110404>.
- [50] W.L. Jorgensen, J. Chandrasekhar, J.D. Madura, R.W. Impey, M.L. Klein, Comparison of simple potential functions for simulating liquid water, *J. Chem. Phys.* 79 (2) (1983) 926–935, <http://dx.doi.org/10.1063/1.445869>.
- [51] A.D. MacKerell, Jr., D. Bashford, M. Bellott, D.R. L., J.D. Evanseck, M.J. Field, S. Fischer, J. Gao, H. Guo, S. Ha, D. Joseph-McCarthy, L. Kuchnir, K. Kuczyra, F.T.K. Lau, C. Mattos, S. Michnick, T. Ngo, D.T. Nguyen, B. Prodhom, W.E. Reiher, B. Roux, M. Schlenkrich, J.C. Smith, R. Stote, J. Straub, M. Watanabe, J. Wiórkiewicz-Kuczyra, D. Yin, M. Karplus, All-atom empirical potential for molecular modeling and dynamics studies of proteins, *J. Phys. Chem. B* 102 (18) (1998) 3586–3616, <http://dx.doi.org/10.1021/jp973084f>, PMID: 24889800.
- [52] S. Del Gaudio, P. Marracino, M. D'Abramo, A. Amadei, In silico characterization of protein partial molecular volumes and hydration shells, *Phys. Chem. Chem. Phys.* 17 (2015) 31270–31277, <http://dx.doi.org/10.1039/C5CP05891K>.
- [53] G. Bussi, D. Donadio, M. Parrinello, Canonical sampling through velocity rescaling, *J. Chem. Phys.* 126 (1) (2007) 014101, <http://dx.doi.org/10.1063/1.2408420>.
- [54] D.M. York, T.A. Darden, L.G. Pedersen, The effect of long-range electrostatic interactions in simulations of macromolecular crystals: A comparison of the Ewald and truncated list methods, *J. Chem. Phys.* 99 (10) (1993) 8345–8348, <http://dx.doi.org/10.1063/1.465608>.
- [55] B. Hess, H. Bekker, H.J.C. Berendsen, J.G.E.M. Fraaije, LINC: A linear constraint solver for molecular simulations, *J. Comput. Chem.* 18 (12) (1997) 1463–1472.
- [56] K. Vanommeslaeghe, E. Hatcher, C. Acharya, S. Kundu, S. Zhong, J. Shim, E. Darian, O. Guvench, P. Lopes, I. Vorobyov, A.D. MacKerell, Jr., CHARMM general force field: A force field for drug-like molecules compatible with the CHARMM all-atom additive biological force fields, *J. Comput. Chem.* 31 (4) (2010) 671–690, <http://dx.doi.org/10.1002/jcc.21367>.
- [57] R.B. Best, X. Zhu, J. Shim, P.E.M. Lopes, J. Mittal, M. Feig, A.D. MacKerell, Optimization of the additive CHARMM all-atom protein force field targeting improved sampling of the backbone ψ , ϕ and side-chain χ_1 and χ_2 Dihedral Angles, *J. Chem. Theory Comput.* 8 (9) (2012) 3257–3273, <http://dx.doi.org/10.1021/ct300400x>, PMID: 23341755.
- [58] M. D'Abramo, M. Aschi, A. Amadei, Theoretical modeling of UV-Vis absorption and emission spectra in liquid state systems including vibrational and conformational effects: Explicit treatment of the vibronic transitions, *J. Chem. Phys.* 140 (16) (2014) 164104, <http://dx.doi.org/10.1063/1.4871626>.
- [59] M. D'Abramo, M. Aschi, A. Amadei, Theoretical calculation of the pyrene emission properties in different solvents, *Chem. Phys. Lett.* 639 (2015) 17–22, <http://dx.doi.org/10.1016/j.cplett.2015.08.070>.
- [60] M. Aschi, V. Barone, B. Carloti, I. Daidone, F. Elisei, A. Amadei, Photoexcitation and relaxation kinetics of molecular systems in solution: towards a complete in silico model, *Phys. Chem. Chem. Phys.* 18 (2016) 28919–28931, <http://dx.doi.org/10.1039/C6CP06167B>.
- [61] M.J. Abraham, T. Murtola, R. Schulz, S. Páll, J.C. Smith, B. Hess, E. Lindahl, GROMACS: High performance molecular simulations through multi-level parallelism from laptops to supercomputers, *SoftwareX* 1–2 (2015) 19–25, <http://dx.doi.org/10.1016/j.softx.2015.06.001>.
- [62] X. Shen, J.R. Knutson, Subpicosecond fluorescence spectra of tryptophan in water, *J. Phys. Chem. B* 105 (26) (2001) 6260–6265, <http://dx.doi.org/10.1021/jp010384v>.
- [63] V.K. Jaiswal, P. Kabaciński, B.E. Nogueira de Faria, M. Gentile, A.M. de Paula, R. Borrego-Varillas, A. Nenov, I. Conti, G. Cerullo, M. Garavelli, Environment-driven coherent population transfer governs the ultrafast photophysics of tryptophan, *J. Am. Chem. Soc.* 144 (28) (2022) 12884–12892, <http://dx.doi.org/10.1021/jacs.2c04565>, PMID: 35796759.
- [64] A. Kowalska-Baron, M. Chan, K. Gałęcki, S. Wysocki, Photophysics of indole, tryptophan and N-acetyl-L-tryptophanamide (NATA): Heavy atom effect, *Spectrochim. Acta A Mol. Biomol. Spectrosc.* 98 (2012) 282–289, <http://dx.doi.org/10.1016/j.saa.2012.08.017>.
- [65] H.B. Steen, Wavelength dependence of the quantum yield of fluorescence and photoionization of indoles, *J. Chem. Phys.* 61 (10) (2003) 3997–4002, <http://dx.doi.org/10.1063/1.1681692>.

- [66] L. Wang, A. Akimov, O.V. Prezhdo, Recent progress in surface hopping: 2011–2015, *J. Phys. Chem. Lett.* 7 (11) (2016) 2100–2112, <http://dx.doi.org/10.1021/acs.jpclett.6b00710>, PMID: 27171314.
- [67] F. Agostini, B.F.E. Curchod, Different flavors of nonadiabatic molecular dynamics, *Wiley Interdiscip. Rev. Comput. Mol. Sci.* 9 (5) (2019) e1417, <http://dx.doi.org/10.1002/wcms.1417>.
- [68] S. Mai, P. Marquetand, L. González, Nonadiabatic dynamics: The SHARC approach, *WIREs Comput. Mol. Sci.* 8 (6) (2018) e1370, <http://dx.doi.org/10.1002/wcms.1370>.
- [69] W. De Lauder, P. Wahl, Effect of solvent upon the fluorescence decay of indole, *Biochim. Biophys. Acta Prot. Struct.* 243 (2) (1971) 153–163, [http://dx.doi.org/10.1016/0005-2795\(71\)90071-7](http://dx.doi.org/10.1016/0005-2795(71)90071-7).
- [70] I. Tatischeff, R. Klein, Influence of the environment on the excitation wavelength dependence of the fluorescence quantum yield of indole, *Photochem. Photobiol.* 22 (6) (1975) 221–229, <http://dx.doi.org/10.1111/j.1751-1097.1975.tb06740.x>.